

## Enhanced Reactive Oxygen Species Generation by Mitochondria Targeting of Anti-cancer Drug to Overcome Tumor Multidrug Resistance

Yuanyuan Liu, Zhou Zhou, Xi Lin, Xiaofeng Xiong, Rui Zhou, Minglu Zhou, and Yuan Huang

*Biomacromolecules*, Just Accepted Manuscript • DOI: 10.1021/acs.biomac.9b00800 • Publication Date (Web): 29 Aug 2019

Downloaded from [pubs.acs.org](https://pubs.acs.org) on August 31, 2019

### Just Accepted

“Just Accepted” manuscripts have been peer-reviewed and accepted for publication. They are posted online prior to technical editing, formatting for publication and author proofing. The American Chemical Society provides “Just Accepted” as a service to the research community to expedite the dissemination of scientific material as soon as possible after acceptance. “Just Accepted” manuscripts appear in full in PDF format accompanied by an HTML abstract. “Just Accepted” manuscripts have been fully peer reviewed, but should not be considered the official version of record. They are citable by the Digital Object Identifier (DOI®). “Just Accepted” is an optional service offered to authors. Therefore, the “Just Accepted” Web site may not include all articles that will be published in the journal. After a manuscript is technically edited and formatted, it will be removed from the “Just Accepted” Web site and published as an ASAP article. Note that technical editing may introduce minor changes to the manuscript text and/or graphics which could affect content, and all legal disclaimers and ethical guidelines that apply to the journal pertain. ACS cannot be held responsible for errors or consequences arising from the use of information contained in these “Just Accepted” manuscripts.

1  
2  
3  
4 **Enhanced Reactive Oxygen Species Generation by Mitochondria**  
5 **Targeting of Anti-cancer Drug to Overcome Tumor Multidrug**  
6 **Resistance**  
7  
8  
9  
10

11 Yuanyuan Liu<sup>#</sup>, Zhou Zhou<sup>#</sup>, Xi Lin, Xiaofeng Xiong, Rui Zhou, Minglu Zhou, Yuan Huang<sup>\*</sup>  
12  
13

14  
15  
16 Key Laboratory of Drug Targeting and Drug Delivery System, Ministry of Education, West China School of  
17 Pharmacy, Sichuan University, No. 17, Block 3, Southern Renmin Road, Chengdu 610041, P. R. China.  
18  
19

20  
21  
22 # These authors contributed equally to this work.  
23

24 \*Phone/fax: +86-28-85501617.  
25

26  
27 E-mail: [huangyuan0@163.com](mailto:huangyuan0@163.com).  
28  
29  
30  
31  
32  
33  
34  
35  
36  
37  
38  
39  
40  
41  
42  
43  
44  
45  
46  
47  
48  
49  
50  
51  
52  
53  
54  
55  
56  
57  
58  
59  
60

## Abstract

As a major clinical tumor chemotherapeutic burden, multidrug resistance (MDR) is often a result of up-regulation of P-glycoprotein (P-gp), which strongly enhance anti-cancer drug efflux. The excess mitochondrial reactive oxygen species (ROS) not only could inhibit the function of P-gp through insufficient adenosine triphosphate supply, but also could cause apoptosis in MDR cells. Here, we designed a mitochondria targeting nanoparticulate system (GNPs-P-Dox-GA) for overcoming MDR through enhanced ROS generation, where increased cellular uptake as well as mitochondria accumulation were both realized by glycyrrhetic acid (GA). Firstly, doxorubicin was conjugated with GA (GA-Dox) and then grafted onto *N*-(2-hydroxypropyl) methacrylamide (HPMA) copolymer backbone via hydrazone bond (P-Dox-GA). The obtained P-Dox-GA was subsequently attached to the surface of gelatin nanoparticles (GNPs). As gelatin is a substrate of tumor extracellular metal matrix protease-2 (MMP2), GNPs-P-Dox-GA nanoparticles could be degraded and release small size P-Dox-GA to facilitate tumor tissue penetration. After P-Dox-GA internalized by tumor cells under GA mediation, Dox-GA detached from HPMA copolymer through hydrolysis of hydrazone bond and then efficiently delivered to mitochondria. Compared to non-GA modified carriers, GNPs-P-Dox-GA exhibited increased cellular uptake nearly for 4-fold and mitochondria distribution for 8.8-fold, and increased ROS production level for nearly 3-fold, significantly decreased efflux rate (55% compared with Dox group) in drug-resistant HepG2/ADR cells, and then led to improved *in vitro* anti-tumor efficiency in HepG2/ADR cells (IC<sub>50</sub> only 19.5% of unmodified ones) as well as exciting *in vivo* anti-tumor efficiency on HepG2/ADR heterotopic tumor nude mice (1.75-fold higher TGIR than free drug).

## Key words

Drug resistance; P-glycoprotein; Mitochondria; Reactive oxygen species; HPMA copolymer; Gelatin nanoparticle

## 1. Introduction

Multidrug resistance (MDR), known as a serious clinical chemotherapeutic problem in effective tumor therapy, is often a result of up-regulation of P-glycoprotein (P-gp).<sup>1, 2</sup> P-gp has been identified to actively promote the efflux of drugs (e.g., doxorubicin, paclitaxel) from cytoplasm before they reach targets and take effect in drug resistant cells.<sup>3, 4</sup> Strenuous efforts have been made to overcome MDR. One strategy is developing drug delivery systems as studies have reported that polymers and nanoparticles can bypass P-gp efflux through endocytosis pathway.<sup>5-7</sup> Another strategy is combining anti-cancer drug with P-gp inhibitor. However, currently their clinical administrations are still challenged mainly due to intolerable toxicity, non-specific action, drug metabolism.<sup>2, 8</sup> Therefore, considerable effort remains to be made to inhibit P-gp function or bypass P-gp efflux for tackling MDR.

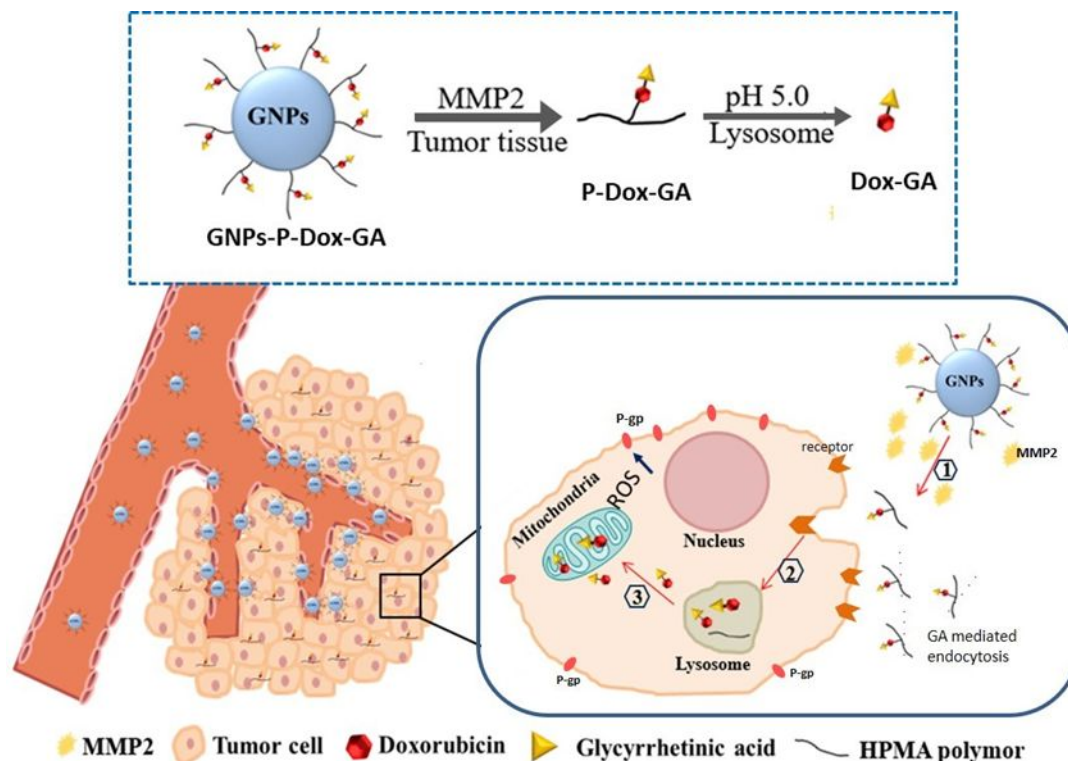
It had been reported that specifically increasing mitochondrial reactive oxygen species (ROS) level can oxidize NADH into NAD<sup>+</sup>, leading P-gp pumps dysfunction through insufficient adenosine triphosphate (ATP) supply, thus rendering resistant cells more susceptible to anticancer drugs.<sup>9</sup> Hence, mitochondrial ROS were selected and widely studied as a promising endogenous P-gp inhibitor for overcoming MDR.<sup>10, 11</sup> Studies have demonstrated that reductive activation of doxorubicin (Dox) aglycone structure results in semiquinone radicals formation in mitochondria, which are strong ROS that can lead to ROS-mediated cell apoptosis. Prospectively, mitochondria targeting delivery of Dox to produce high level of ROS potentially offers an opportunity to overcome MDR.

*N*-(2-hydroxypropyl) methacrylamide (HPMA) copolymer, is a promising small-sized carrier due to its biocompatibility, good tumor penetration and increase of hydrophobic drug solubility.<sup>12, 13</sup> Our previous studies had demonstrated that HPMA copolymers with a size of 10-20 nm could achieve deep tumor penetration,<sup>14</sup> meanwhile their *in vivo* delivery and tumor accumulation efficiency could be further improved after the size of copolymer enlarged by being prepared to micelles or conjugated onto a nanoparticle core.<sup>15-18</sup> Gelatin is a metal matrix protease-2 (MMP2) substrate which overexpressed in tumors.<sup>19, 20</sup> Our another previous study had demonstrated that gelatin nanoparticles (GNPs) were stable in blood circulation and quickly degraded by extracellular MMP2 once accumulated in hepatocellular tumor, leading to small amphiphilic prodrug release, followed by penetrated deeply into tumor tissues.<sup>21</sup> Based on these results, HPMA copolymer modified GNPs would be a desirable carrier for mitochondria targeting of anti-tumor prodrug.

To achieve mitochondria targeting delivery, mitochondria-targeting signal peptides and lipophilic cations (e.g., triphenylphosphonium, dequalinium) have been used.<sup>22-24</sup> However, as some mitochondria targeting groups do not have significant tumor cell targeting ability or can not enhance cellular uptake of drugs, the

1  
2  
3 simultaneous use of cell targeting peptide or cell penetrating peptide as well as mitochondria targeting ligand in  
4 drug delivery systems was developed.<sup>25</sup> Another strategy is to use ligand which is able to increase both cellular  
5 uptake and mitochondria targeting.<sup>26</sup> Glycyrrhetic acid (GA) is capable of specifically recognizing protein kinase  
6 C  $\alpha$ , which highly expressed in hepatocellular carcinoma (HCC) cells.<sup>27-29</sup> More importantly, recently it was  
7 reported that GA-functionalized graphene oxide significantly enhanced drug distribution in mitochondria.<sup>30</sup>  
8 Therefore, GA has great potential as a sequential-targeting ligand from cell membrane to mitochondria. However,  
9 it remains challenging for GA-conjugated nanoparticles achieving mitochondria targeting due to the outer  
10 mitochondrial membrane only allow passage of molecules less than 5 KDa.<sup>31</sup> Hence, smart drug delivery system  
11 which can release mitochondria targeting GA-drug conjugates after tumor cell internalization should be  
12 developed.  
13  
14  
15  
16  
17  
18

19  
20 Herein, we proposed a sequential tumor cell targeting and mitochondria targeting delivery system (GNPs-P-  
21 Dox-GA) for overcoming MDR through ROS generation. Firstly, doxorubicin was conjugated with GA (GA-Dox) and  
22 then grafted onto HPMA copolymer backbone via hydrazone bond (P-Dox-GA). The obtained P-Dox-GA was  
23 subsequently attached to the surface of gelatin nanoparticles (GNPs) (Scheme 1). The GNPs-P-Dox-GA  
24 nanoparticles would stay stable in blood circulation, and then degraded by tumor extracellular MMP2 and release  
25 smaller size P-Dox-GA to facilitate tumor tissue penetration. After P-Dox-GA internalized by tumor cells under  
26 GA mediation and delivered to lysosomes, Dox-GA detached from HPMA copolymer through hydrolysis of  
27 hydrazone bonds and then efficiently delivered to mitochondria. Then, a large number of ROS would be produced  
28 by mitochondria damage, causing dysfunction of P-gp pumps and cell apoptosis for overcoming MDR. In this  
29 study, cellular uptake, mitochondria distribution, ROS product efficacy, P-gp activities, as well as anti-tumor  
30 effects on MDR tumor were investigated. GA modification was used as a “one stone two birds” strategy for  
31 realizing effective cellular uptake as well as mitochondria targeting. Besides, this study gives insights into  
32 overcoming MDR through enhanced ROS generation in mitochondria, not only inhibit drug efflux but also cause  
33 apoptosis on MDR cells.  
34  
35  
36  
37  
38  
39  
40  
41  
42  
43  
44  
45  
46  
47  
48  
49  
50  
51  
52  
53  
54  
55  
56  
57  
58  
59  
60



**Scheme 1.** (1) Triggered by tumor extracellular metal matrix protease-2 (MMP2), small size HPMA copolymer P-Dox-GA released from gelatin nanoparticles GNP-P-Dox-GA, facilitating tumor tissue penetration. (2) After internalized by tumor cells under the mediation of GA and delivered to lysosomes, small-molecular Dox-GA detached from HPMA copolymer through hydrolysis of hydrazone bonds and (3) then efficiently delivered to mitochondria, where extensive reactive oxygen species (ROS) produced by mitochondria damage, causing dysfunction of P-glycoprotein pumps and ROS-mediated cell apoptosis for overcoming multidrug resistance.

## 2. Materials and Methods

### 2.1 Materials

Gelatin (type A), 3-(4,5-dimethyl-2-tetrazolyl)-2,5-diphenyl-2H tetrazoliumbromide (MTT), 4',6-diamidino-2-phenylindole (DAPI) were purchased from Sigma-Aldrich (St. Louis, MO, USA). Doxorubicin hydrochloride (Dox·HCl) was from Dalian Meilun Biotech Co., Ltd. (Dalian, China). BCA Protein Assay Kit, Cell Mitochondria Isolation Kit and Reactive Oxygen Species Assay Kit were purchased from Beyotime Institute of Biotechnology (China). MitoTracker Green was purchased from Invitrogen (Carlsbad, CA, USA). Glycyrrhetic acid was got from J&K Co., Ltd. (Shanghai, China). Comonomer HPMA<sup>32</sup> and *N*-methacryloylglycylglycyl-hydrazide-doxorubicin (MA-GG-NHN=Dox)<sup>16</sup> were obtained by previous synthetic methods.

## 2.2 Synthesis of HPMA copolymers

### 2.2.1 Synthesis of initiator ABIK-PDS

2-(2-pyridyldithio) ethylamine hydrochloride (PDEA, 17.1 mmol, synthetic details were described in supplementary materials) and 4,4'-Azobis (4-cyanovaleric acid) (ABIK, 8.53 mmol) were dispersed in chloroform (100 mL). To this suspension, triethylamine (17.1 mmol) was added under vigorous stirring to form a clear solution. Subsequently, dicyclohexylcarbodiimide (DCC, 20.3 mmol) was added slowly to the reaction mixture, which was kept stirring for 24 h. The mixture was concentrated and purified by silica-gel column chromatography (ethyl acetate) to afford ABIK-PDS in a yield of 66.4%. <sup>1</sup>H NMR spectra and mass spectra were conducted to identify the product.

### 2.2.2 Synthesis of glycyrrhetic acid derivative suc-GA

Glycyrrhetic acid (2.5 mmol), succinyl anhydride (10.0 mmol) and 4-dimethylaminopyridine (DMAP, 5.0 mmol) were dissolved in dichloromethane (DCM). The reaction mixture was refluxed for 12 h, then washed with saturated sodium chloride solution. The organic layer was concentrated and recrystallized in ethanol to afford the glycyrrhetic acid derivative (suc-GA) in a yield of 67.8%. <sup>1</sup>H NMR spectra and mass spectra were conducted to identify the product.

### 2.2.3 Synthesis of HPMA copolymers

The telechelic HPMA copolymer doxorubicin conjugate with a thiol end group (P-Dox) was synthesized by its precursor HPMA copolymer doxorubicin conjugate containing 2-pyridyldisulfanyl (PDS) terminal (P-Dox-PDS). Firstly, P-Dox-PDS was synthesized by radical solution polymerisation in dimethylsulfoxide (initiator ABIK-PDS, 5 wt%; monomer 12.5 wt%; HPMA and MA-GG-NHN=Dox in a molar ratio of 70 to 30). The mixture was reacted under nitrogen for one day (70°C, in dark). The reaction mixture was precipitated in acetone. The precipitate was redissolved in water and filtered by 0.22 µm microporous membrane. The filtrate was dialysed against deionized water for 24 h and freeze-dried to afford the HPMA copolymer precursor P-Dox-PDS in a yield of 66.2%. Then, the obtained P-Dox-PDS was dissolved in dithiothreitol solution (DTT, 0.1 M) which was gently stirred at room temperature. The reaction lasted for 30 min, then the mixture was dialysed against deionized water for two days, filtered (0.22 µm) and freeze-dried. The desired telechelic copolymer was obtained in a yield of 89.2%.

HPMA copolymer glycyrrhetic acid derivative conjugate containing a thiol end group (P-Dox-GA) was synthesized by two steps. Firstly, glycyrrhetic acid derivative suc-GA (0.276 mmol) was completely dissolved in *N,N*-dimethylformamide. *N*-hydroxysuccinimide (NHS, 0.414 mmol) and 1-(3-dimethylaminopropyl)-3-

ethylcarbodiimide hydrochloride (EDC·HCl, 0.414 mmol) were added subsequently to the solution. After 3 hours' activation, the reaction mixture was added with previously synthesized P-Dox (0.092 mmol Dox equivalent). The solution was stirred for 24 h in dark before being dialyzed against deionized water for 2 days. After filtration (0.22  $\mu\text{m}$ ) and freeze-drying, the copolymer P-Dox-GA was obtained in a yield of 63.0%.

## 2.3 Preparation of gelatin nanoparticles

### 2.3.1 Synthesis of 3-(2-pyridyldithio) propionic acid *N*-hydroxy-succinimide ester (SPDP)

2,2'-Dipyridyldisulfide (3.75 g) and glacial acetic acid (400  $\mu\text{L}$ ) was dissolved in methanol. 3-mercaptopropionic acid (0.9 g in 5 mL methanol) was added dropwise to this solution. After 24 h reaction, the solution was concentrated and separated by alumina column chromatography (dichloromethane/ethanol = 2/3, v/v). Eluent containing the product was collected and concentrated. The residue was recrystallized in ethyl acetate/hexane to afford the product as a pale solid. Then 5.0 mmol of the obtained product was dissolved in DCM. The solution was added with NHS (7.5 mmol) and DCC (7.5 mmol) subsequently and reacted for 4 h, then kept in 4°C overnight without stirring. The precipitation, dicyclohexylurea (DCU), was removed by filtration and the filtrate was concentrated. The residue was recrystallized in ethanol to afford the product as a white solid.  $^1\text{H}$  NMR spectra and mass spectra were conducted to identify the product (SPDP).

### 2.3.2 Preparation of GNPs-P-Dox-GA and GNPs-P-Dox

P-Dox-GA modified gelatin nanoparticles GNPs-P-Dox-GA were prepared by two steps. Firstly, gelatin nanoparticles (GNPs) were prepared as previously described.<sup>21</sup> The GNPs solution (20 mg/mL, 4 mL) was adjusted to pH 8.0, followed by the addition of SPDP (8 mg in dimethylformamide). After 24 h's reaction, unreacted SPDP was removed by dialysis (dimethylformamide/phosphate buffer solution: 1/4 for one day, phosphate buffer solution for another day). Then gelatin nanoparticles with PDS terminal (GNPs-PDS) were harvested as solution. Secondly, the above GNPs-PDS solution (20 mg/mL, 4 mL) was adjusted to pH 6.0 and added with P-Dox-GA (0.015 mmol thiol group equivalent). 8 hours later, the mixture was dialyzed against phosphate buffer solution for two days to afford the GNPs-P-Dox-GA solution. P-Dox modified gelatin nanoparticles GNPs-P-Dox was prepared as a control by the same procedure.

## 2.4 Characterization of gelatin nanoparticles and HPMA copolymers

The hydrate size as well as zeta potential of gelatin nanoparticles and HPMA copolymers were characterized by Zetasizer Nano ZS90 (Malvern, UK). GNPs-P-Dox-GA morphology was imaged by transmission electron microscopy (TEM, H-600, Hitachi, Japan). Thiol group content in HPMA copolymers and PDS content on gelatin nanoparticle GNPs-PDS were measured as previously reported.<sup>18</sup> Dox loading in HPMA copolymers and

1  
2  
3 nanoparticles were quantified by UV-Vis analysis at 487 nm. For stability study, GNPs-P-Dox-GA size was  
4 characterized in pH 7.4 phosphate buffer solution (PBS) by dynamic light scattering (DLS) at predetermined time  
5 points.  
6  
7

## 8 **2.5 *In vitro* drug release**

10  
11 The dialysis method was used to evaluate the release profile of Dox-GA from GNPs-P-Dox-GA. GNPs-P-Dox-  
12 GA (0.4 mg/mL, 3 mL) was sealed into a dialysis bag (MWCO 3000), followed by incubation with buffer solution  
13 under various pH conditions at 37°C (pH 7.4 mimicking physiological condition, pH 6.5 mimicking tumor  
14 microenvironment and pH 5.0 mimicking lysosome environment). At scheduled intervals, 200 µL of buffer solution  
15 was collected from the outer phase of the dialysis bag, and replaced with 200 µL of fresh buffer solution. The  
16 drug concentration was calculated by the fluorescence intensity of Dox (Ex=487nm, Em=533nm) measured by  
17 Varioskan Flash Multimode Reader (Thermo Fisher Scientific, MA, USA).  
18  
19  
20  
21  
22

## 23 **2.6 Cell lines and mice**

24  
25 Human hepatoma cell line (HepG2) and multiple drug resistant HepG2/adriamycin cell line (HepG2/ADR)  
26 were both cultured in RPMI 1640 medium (37°C, 5% CO<sub>2</sub>), supplemented with 10% fetal bovine serum and 1%  
27 penicillin (100 IU/mL)/streptomycin (100 µg/mL). The culture medium of HepG2/ADR was supplemented with  
28 doxorubicin (0.5 µg/mL) to maintain the drug resistant phenotype.  
29  
30  
31

32  
33 Male BALB/c nude mice (4-6 weeks) were obtained from Chengdu Dashuo Biological Technology Co., Ltd.  
34 (Chengdu, China). All the mice were housed under the guidelines of Sichuan University.  
35  
36

## 37 **2.7 Cellular uptake**

38  
39 HepG2 and HepG2/ADR cell were seeded on 6-well plates (1×10<sup>5</sup> cells/well). After 24 h, cells were treated  
40 with a series of gelatin nanoparticles and HPMA copolymers at an equivalent dose (Dox: 10 µg/mL) for 1 h or 4  
41 h. Next, cells were washed thrice with fresh PBS. The extracellular fluorescence was quenched using trypan blue  
42 (0.4%). Then, cells were incubated with RIPA lysis buffer and collected. After centrifugation (3000 rpm, 3 min),  
43 the supernatant was obtained and the total protein in each sample was measured by BCA protein assay kit.<sup>33, 34</sup>  
44 The fluorescence intensity of Dox was detected as described above.  
45  
46  
47  
48  
49

50 For confocal laser scanning microscope (CLSM) imaging, HepG2/ADR cells were cultured on glass c  
51 overslips for 24 h. Cells were then treated with gelatin nanoparticles and HPMA copolymers for 4 h  
52 at an equivalent dose (10 µg/mL Dox). After rinsed thrice with PBS, cells were fixed with 4% formald  
53 ehyde, and stained by 4',6-diamidino-2-phenylindole (DAPI). Finally, cells were visualized by CLSM (LSM  
54  
55  
56  
57

1  
2  
3 800, Zeiss, Germany).

## 4 5 **2.8 Mitochondria targeting**

6  
7 For quantitative analysis of mitochondria targeting, HepG2/ADR cells were cultured in 6-well plates ( $1 \times 10^5$   
8 cells/well), then treated with gelatin nanoparticles and HPMA copolymer conjugates for 1 h or 4 h at an  
9 equivalent dose (Dox:  $10 \mu\text{g}/\text{mL}$ ). Cells were collected after washing with fresh PBS thrice. Mitochondria obtained  
10 by Cell Mitochondria Isolation Kit were lysed by incubation with mitochondria lysis buffer. After centrifugation  
11 (10000  $g \diamond 10$  min,  $4^\circ\text{C}$ ), total protein in the collected supernatants were immediately detected by a BCA protein  
12 assay kit. The fluorescence intensity of Dox was detected as described above.  
13  
14  
15  
16  
17

18 For CLSM imaging, HepG2/ADR cells ( $1 \times 10^4$  cells/well) were cultured for 24 h on glass coverslips. After  
19 exposure to gelatin nanoparticles and HPMA copolymer conjugates for 4 h at an equivalent dose (Dox:  $10 \mu\text{g}/\text{mL}$ ),  
20 cells were stained with MitoTracker green ( $100 \text{ nM}$ ) and DAPI. Finally, cells were observed using CLSM.  
21  
22  
23  
24  
25

## 26 **2.9 ROS level**

27  
28 HepG2/ADR cells ( $2 \times 10^5$  cells/well) were cultured in 12-well plates. After exposure to gelatin nanoparticles  
29 and HPMA copolymer conjugates for 4 h at an equivalent dose (Dox:  $10 \mu\text{g}/\text{mL}$ ), cells were washed and collected.  
30 The ROS level was determined by Reactive Oxygen Species Assay Kit and flow cytometer according to the  
31 instructions.  
32  
33  
34  
35

## 36 **2.10 P-glycoprotein activities**

37  
38 HepG2/ADR cells ( $1 \times 10^5$  cells/well) were cultured for 24 h in 24-well plates. Cells were then treated with  
39 gelatin nanoparticles and HPMA copolymer conjugates at an equivalent dose (Dox:  $10 \mu\text{g}/\text{mL}$ ) for 4 h. Then the  
40 medium was replaced by calcien AM ( $0.2 \mu\text{M}$ ). After 30 min, cells were washed and lysed using RIPA lysis buffer.  
41 After centrifugation (3000 rpm  $\diamond 10$  min,  $4^\circ\text{C}$ ), the total protein in the collected supernatant was detected as  
42 described above, The fluorescence intensity of calcien AM in supernatants was determined *via* Varioskan Flash  
43 Multimode Reader.  
44  
45  
46  
47  
48

## 49 **2.11 Drug efflux assay**

50  
51 HepG2/ADR cells ( $1 \times 10^5$  cells/well) were cultured for 24 h on 24-well plates. After treated with gelatin  
52 nanoparticles and HPMA copolymer conjugates at an equivalent dose (Dox:  $10 \mu\text{g}/\text{mL}$ ) for 4 h, the cells were  
53 then treated with fresh RPMI-1640 medium for another 4 h. Afterwards, extracellular fluorescence was  
54  
55  
56  
57  
58  
59  
60

1  
2  
3 quenched with trypan blue (0.4%) and the cells were lysed by RIPA buffer incubation. After centrifugated (3000  
4 rpm  $\times$  10 min, 4°C), the total protein and fluorescence intensity of Dox in the collected supernatant were detected  
5 as described above. Drug efflux ratio was calculated by the following formula: efflux ratio =  $(C_A - C_B)/C_A \times 100\%$ , ( $C_A$ ,  
6 fluorescence intensity of cell treated with sample for 4 h;  $C_B$ , fluorescence intensity of cell cultured for another  
7 4 h with fresh medium after drug incubation).  
8  
9  
10

### 11 **2.12 *In vitro* antitumor effect**

12  
13  
14 MTT assay was performed to determine the cytotoxicity. HepG2 cells and HepG2/ADR cells were cultured in  
15 96-well plates ( $4 \times 10^3$  cells/well) for 24 h, then treated with gelatin nanoparticles and HPMA copolymer  
16 conjugates for 48 h. Subsequently, the medium was replaced by fresh medium (180  $\mu$ L/well) and 5 mg/mL MTT  
17 solution (5 mg/mL, 20  $\mu$ L/well). After 4 h incubation, the medium was replaced by dimethyl sulfoxide (150  $\mu$ L/well)  
18 and vibrated. Absorbance was assayed *via* Varioskan Flash Multimode Reader at 570 nm.  
19  
20  
21  
22

23 Apoptosis was detected by FITC-Annexin V Apoptosis Kit (BioLegend, USA). In brief, HepG2/ADR cells ( $1 \times 10^5$   
24 cells/well) were treated with various HPMA copolymer conjugates and gelatin nanoparticles (equivalent to 2  
25  $\mu$ g/mL Dox) for 24 h. Cells were rinsed thrice with PBS, then resuspended in binding buffer (100  $\mu$ L) containing  
26 2.5  $\mu$ L annexin-V and 2.5  $\mu$ L 7-amino-actinomycin D, and incubated for 15 min. After addition with 400  $\mu$ L binding  
27 buffer, the cell apoptosis was immediately monitored by flow cytometry.  
28  
29  
30  
31

### 32 **2.13 *In vivo* antitumor effect and histopathological analysis**

33  
34 HepG2/ADR cells ( $1 \times 10^6$  cells) were injected into mice right axilla subcutaneously. Mice were divided into six  
35 groups randomly after HepG2/ADR xenograft tumor volume reached 100 mm<sup>3</sup>. Then saline or samples (2.5 mg/kg  
36 Dox equivalent) were injected *via* tail vein on predetermined days. The body weight and tumor size were  
37 recorded every two days. Tumor size was calculated following the formula:  $V = (L \times W^2)/2$ .  
38  
39  
40  
41

42 After mice sacrificed, main organs and tumors were collected and fixed in 10% formalin, then embedded in  
43 paraffin blocks and cut into slices (4  $\mu$ m). Tumors were stained with hematoxylin and eosin (H&E) and TUNEL  
44 apoptosis assay kit (Roche). Other organs were only performed with H&E staining.  
45  
46  
47

### 48 **2.14 Statistical analysis**

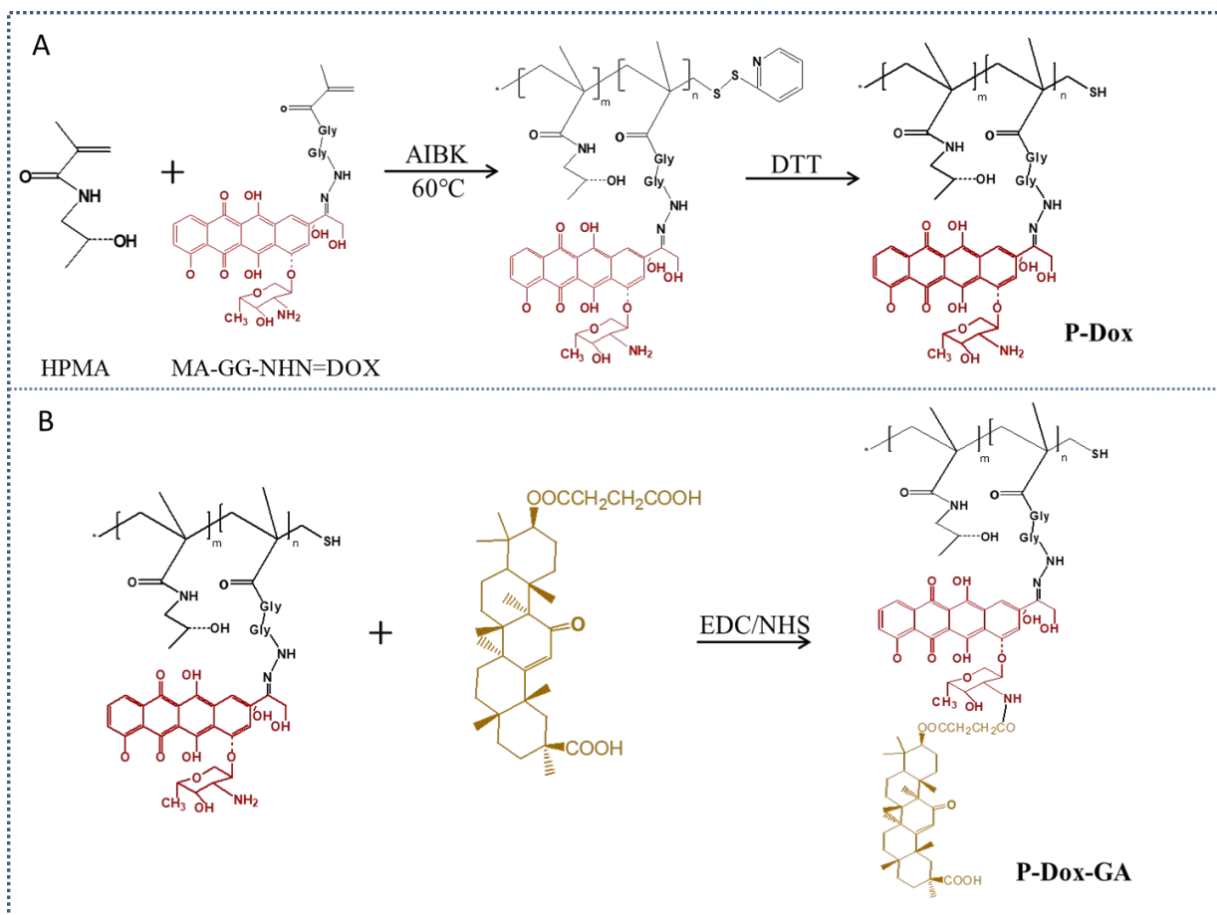
49  
50 Data were mean values  $\pm$  standard deviations (SDs). Statistical analysis was performed using SPSS 17.0  
51 software to execute a two-tailed Student's t-test. *P* value < 0.05 was considered statistically significant.  
52  
53  
54  
55  
56  
57  
58  
59  
60

### 3. Results and Discussion

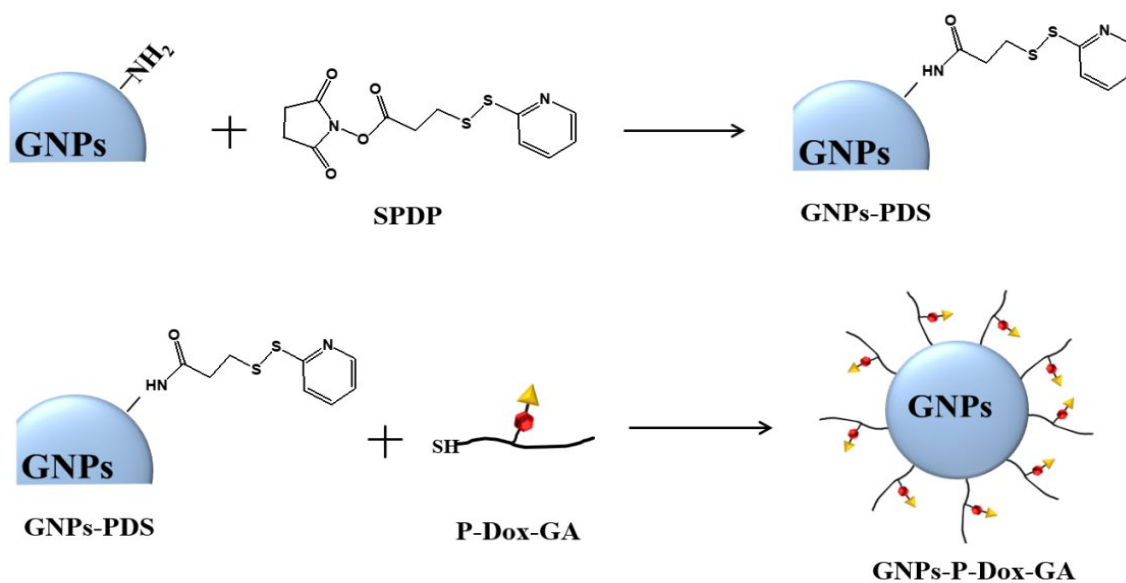
#### 3.1 Characterization of gelatin nanoparticles and HPMA copolymer conjugates

Considering C30-carboxyl group in glycyrrhetic acid (GA) was an active site,<sup>35, 36</sup> which could recognize protein kinase C  $\alpha$  on tumor cell membrane, succinate-GA (suc-GA, Figure S1) was synthesized by introducing another carboxyl group to C3-hydroxyl group.<sup>37, 38</sup> Then comonomers of HPMA copolymer (HPMA, MA-GG-NHN=Dox), PDEA (Figure S2), ABIK-PDS (Figure S3) and HPMA conjugates (P-Dox, P-Dox-GA) were obtained (Scheme 2). The Dox loading of P-Dox-GA and P-Dox was 8.67 wt% and 9.28 wt%, respectively. Hydrate size of P-Dox-GA and P-Dox was 18.61 nm and 15.09 nm respectively (Table 1). Zeta potential of P-Dox-GA (+9.86 mV) was distinctly lower when compared to P-Dox (+20.23 mV), indicating the successful modification of GA.

Gelatin nanoparticles (GNPs-P-Dox, GNPs-P-Dox-GA) were synthesized by two steps (Scheme 3). Firstly, pyridyldisulfanyl (PDS) functionalized GNPs (GNPs-PDS) were obtained by aminolysis of the active ester of SPDP with amino groups on GNPs. After PDS modification, the PDS loading of GNPs-PDS was 0.187 mmol/g. Meanwhile, zeta potential changed from -10.53 mV (GNPs) to -27.92 mV (GNPs-PDS) (Table S1). Secondly, thiol-terminated P-Dox-GA was grafted to GNPs-PDS to form GNPs-P-Dox-GA. Hydrate size of GNPs-P-Dox-GA and GNPs-P-Dox was 111.1 nm and 106.5 nm respectively (Table 1, Figure 1B), with an increase of 10-20 nm compared to GNPs-PDS which was not covered by HPMA copolymers, suggesting the successful modification of HPMA copolymers. TEM result also exhibited that GNPs-P-Dox-GA had a core-shell structure (Figure 1A). All data clearly verified the successful preparation of polymer grafted nanoparticles. Stability analysis of polymer grafted nanoparticle (GNPs-P-Dox-GA) was determined in PBS (pH 7.4). The hydrated



32 **Scheme 2.** Synthesis of HPMA copolymers P-Dox (A) and P-Dox-GA (B).



55 **Scheme 3.** Synthesis of HPMA copolymer modified gelatin nanoparticles GNP-P-Dox-GA.

5  
6  
7  
8  
9  
10  
11  
12  
13  
14  
15  
16  
17  
18  
19  
20  
21  
22  
23  
24  
25  
26  
27  
28  
29  
30  
31  
32  
33  
34  
35  
36  
37  
38  
39  
40  
41  
42  
43  
44  
45  
46  
47  
48  
49  
50  
51  
52  
53  
54  
55  
56  
57  
58  
59  
60

**Table 1.** Characteristics of HPMA copolymers and gelatin nanoparticles (mean  $\pm$  SD, n = 3).

Carriers	Size (nm)	PDI	Zeta potential (mV)	Thiol group (-SH) loading (mmol/g NPs)	Dox loading (wt%)
P-Dox	15.09 $\pm$ 2.11	/	20.23 $\pm$ 2.61	0.10	9.28
P-Dox-GA	18.61 $\pm$ 2.51	/	9.86 $\pm$ 1.62	0.09	8.67
GNPs-P-Dox	106.5 $\pm$ 3.1	0.251 $\pm$ 0.073	-9.87 $\pm$ 2.14	/	5.7
GNPs-P-Dox-GA	111.1 $\pm$ 2.7	0.276 $\pm$ 0.058	-13.92 $\pm$ 2.02	/	5.1

Abbreviations: PDI, polydispersity index; Dox, doxorubicin;

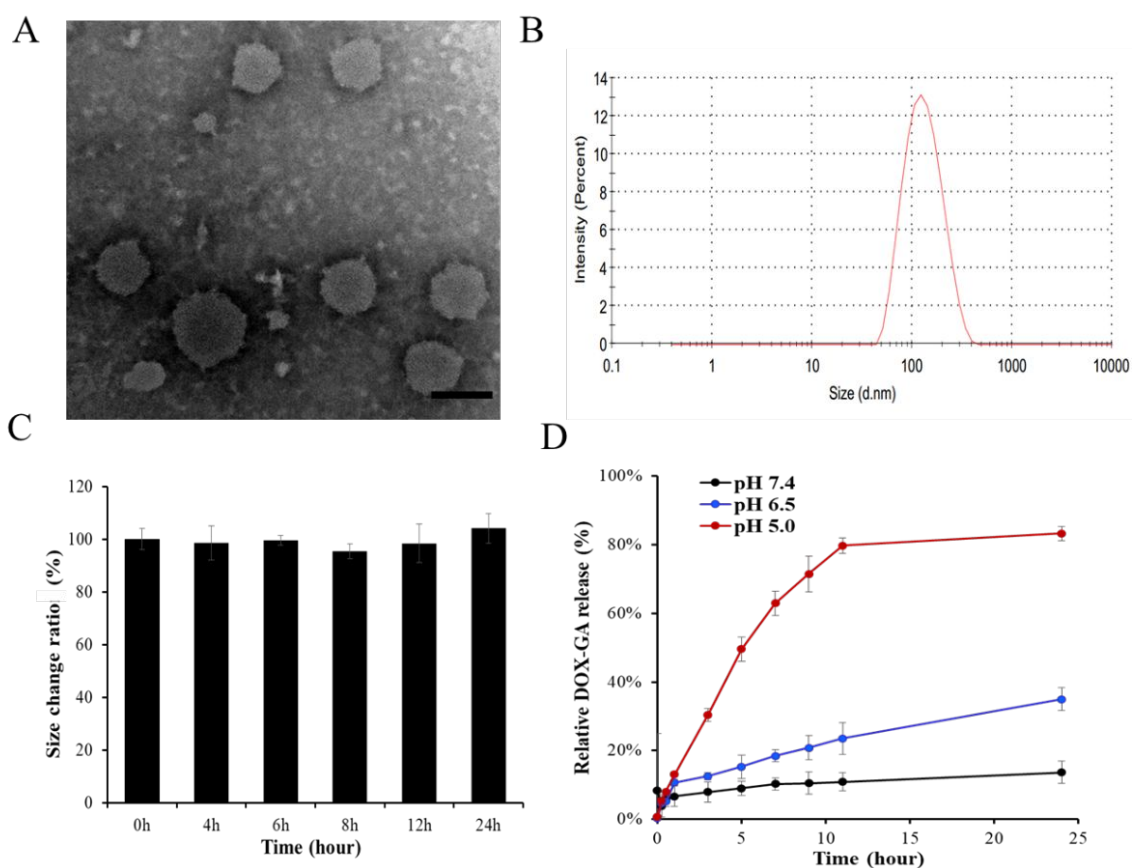


**Figure 1.** (A) Transmission electron micrograph images of GNPs-P-Dox-GA. The scale bar was 100 nm. (B) Hydrate size of GNPs-P-Dox-GA measured by dynamic light scattering. (C) Stability of GNPs-P-Dox-GA in PBS (pH7.4). (D) Dox-GA release from GNPs-P-Dox-GA in PBS under various pH conditions at 37°C.

1  
2  
3 size did not change obviously during 24 h incubation (Figure 1C), implying that GNPs-P-Dox-GA were stable  
4 enough for a long *in vivo* circulation.  
5

### 6 7 **3.2 *In vitro* drug release**

8  
9 It was reported outer mitochondrial membrane (OMM) only allows passage of molecules which are lower  
10 than 5 KDa. Therefore, the release of Dox-GA (1.1 KDa) from GNPs-P-Dox-GA after endocytosis is the prerequisite  
11 for mitochondria accumulation. Hence, Dox-GA release behavior at various pH buffered conditions (pH 7.4  
12 mimicking physiological condition, pH 6.5 mimicking tumor microenvironment and pH 5.0 mimicking lysosome  
13 environment) were determined. In Figure 1D, after 24 h, only a small proportion of Dox-GA released at pH 7.4  
14 (12.3%) or pH 6.5 (26.5%). Inversely, 85.0% of Dox-GA released at pH 5.0. These results suggested that low pH  
15 environment could accelerate Dox-GA release due to hydrolysis of hydrazone in acidic condition. Therefore,  
16 GNPs-P-Dox-GA owned relative stability under physiological environment but could sharply release Dox-GA in  
17 lysosome.  
18  
19  
20  
21  
22  
23

### 24 25 **3.3 Enhanced cellular uptake by GA**

26  
27 Cellular uptake in HepG2 (HCC cell line) and HepG2/ADR (multiple drug-resistant HepG2/adriamycin cell line)  
28 cells was quantified by BCA kit and imaged by CLSM. GA modified groups (P-Dox-GA and GNPs-P-Dox-GA) showed  
29 much higher internalization in both HepG2 (Figure S5, Table S3 and Table S4) and HepG2/ADR cells (Figure 2,  
30 Table S5 and Table S6). Meanwhile, as incubation time prolonged, the internalization of GA-modified carriers (P-  
31 Dox-GA and GNPs-P-Dox-GA) increased significantly in both HepG2 and HepG2/ADR cells, whereas unmodified  
32 groups did not increase, indicating that advantages of GA modification would be more remarkable with  
33 prolonged incubation time. Besides, compared with that of non-GA modified groups, the cellular uptake of P-Dox-  
34 GA had only approximately 2.84-fold improvement in HepG2 cells (Figure S5B), whereas achieving 4.41-fold  
35 increase in HepG2/ADR cells (Figure 2B), which suggested that GA has a stronger role of enhancing cellular uptake  
36 in drug resistant cells.  
37  
38  
39  
40  
41  
42  
43  
44  
45  
46  
47  
48  
49  
50  
51  
52  
53  
54  
55  
56  
57  
58  
59  
60

CLSM of HepG2/ADR cells (Figure 3C) showed similar results. Much stronger red fluorescence was observed in GA modified groups (P-Dox-GA and GNPs-P-Dox-GA) compared with carriers without GA modification. The results indicated that GA modification could enhance the internalization by HepG2/ADR cells. Furthermore, subcellular distribution of these groups was obviously different. In P-Dox-GA and GNPs-P-Dox-GA groups, there was no coincide of blue nuclei and red Dox. In contrast, bright purple area existed in P-Dox and GNPs-P-Dox groups, indicating the distribution of Dox in nuclei. The results suggested that GA could change the subcellular distribution of Dox.

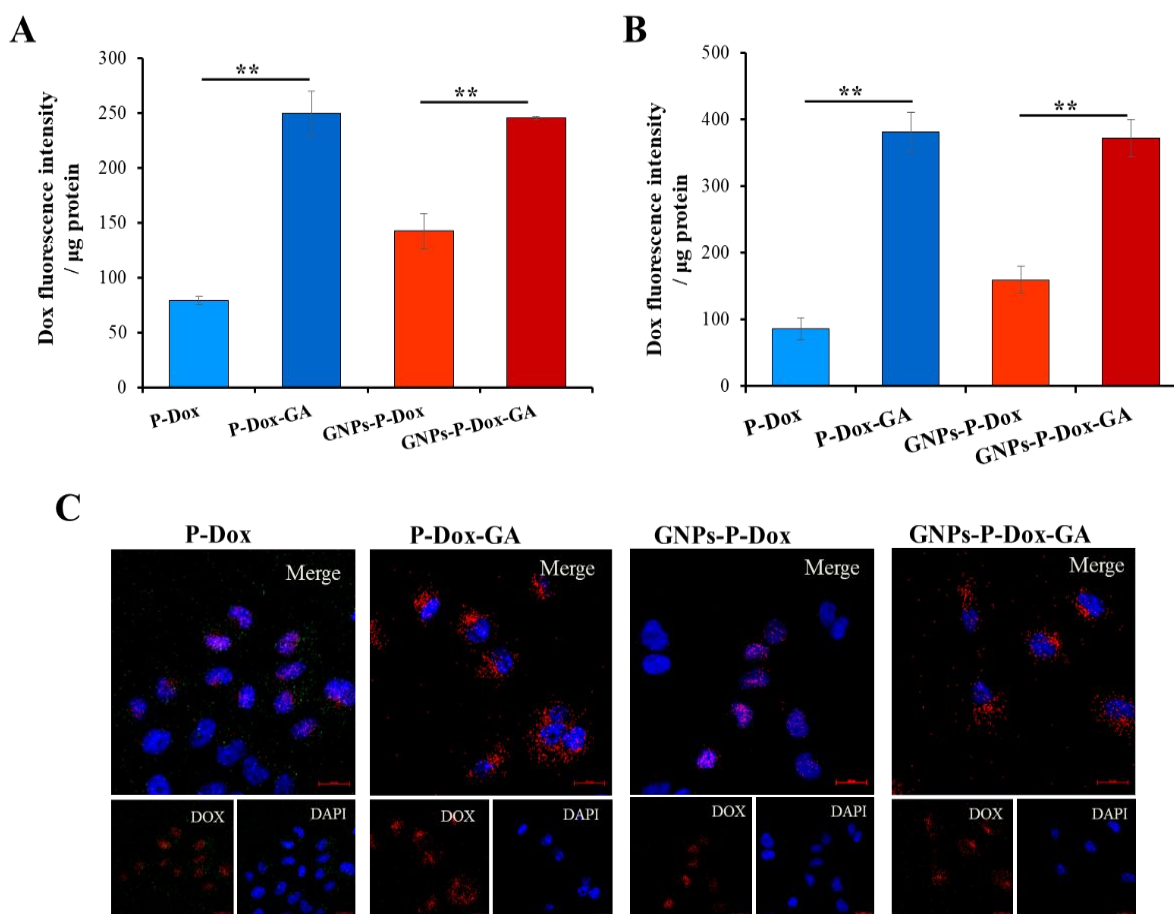


**Figure 2.** Cell internalization in HepG2/ADR cells for (A) 1 h and (B) 4 h.  $**p < 0.01$ . (C) Cellular uptake in HepG2/ADR cells imaged by CLSM after 4 h treatment. Blue fluorescence presented nuclei. Red fluorescence presented Dox.

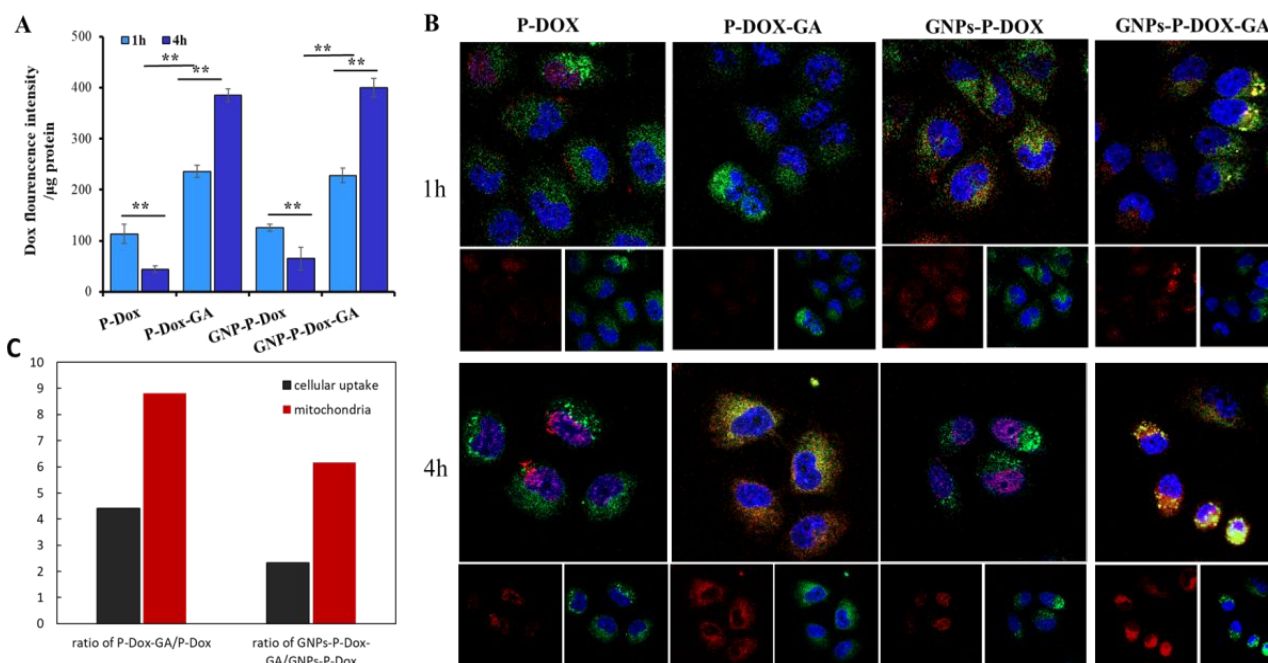


**Figure 3.** (A) Mitochondria targeting in HepG2/ADR cells.  $**p < 0.01$ . (B) Mitochondria colocalization of carriers by CLSM in HepG2/ADR cells. Red fluorescence: Dox. Green fluorescence: mitochondria stained by MitoTracker Green. Blue fluorescence: nuclei stained by DAPI. Yellow fluorescence indicates the colocalization of green mitochondria and red Dox. (C) The ratio of GA modified carriers increased in cellular uptake and mitochondria targeting to unmodified ones.

### 3.4 Improved mitochondria targeting by GA

Dox-GA was released after the hydrolyzation of hydrazone bond between Dox-GA and HPMA polymer backbone. Mitochondria targeting ability of Dox-GA was analyzed qualitatively and quantitatively. Fluorescence intensities in the mitochondria of cells treated with GA modified groups were significantly stronger than that treated with unmodified ones (Figure 3A), indicating GA modification indeed enhanced mitochondria accumulation of Dox. It should be noted that, GA modification led to 6.2-8.8 folds increase in mitochondria accumulation compared to the unmodified counterparts in 4 h incubation, while only 2.3-4.4 folds increase was achieved in the cellular uptake (Figure 3C), suggesting that the increased mitochondrial accumulation was not only owing to the enhanced internalization, but also due to the effective mitochondria targeting ability introduced by GA modification. Besides, mitochondrial distribution of GA modified groups showed significant

1  
2  
3 improvement (1.63-1.75 folds) with prolonged incubation time from 1 h to 4 h. However, in contrast, P-Dox and  
4 GNP-P-Dox groups showed significantly reduced mitochondrial distribution from 1 h to 4 h. This may be on one  
5 hand due to the fact that the cellular uptake of the GA unmodified groups in the drug-resistant cells did not  
6 increase significantly with prolonged incubation time; on the other hand, the Dox mitochondrial distribution was  
7 reduced due to its nuclear tropism. This result also indicated that GA modification can effectively change the  
8 subcellular distribution of Dox.  
9  
10  
11  
12

13  
14 Fluorescence from CLSM also showed similar results to quantitative experiments (Figure 3B). For groups  
15 without GA modification (P-Dox and GNP-P-Dox), the green fluorescence of mitochondria hardly overlapped  
16 with the red fluorescence of Dox; while for GA modified groups (P-Dox-GA and GNP-P-Dox-GA), large areas of  
17 yellow fluorescence, representing the co-localization of mitochondria and Dox, were observed obviously.  
18 These results indicated that Dox-GA possessed effective mitochondria targeting ability.  
19  
20  
21  
22

### 23 **3.5 Increased ROS generation**

24  
25 ROS have been involved in important developmental approach regulation, such as protein-protein  
26 interactions. As a mutagenic agent, ROS can either block self-renewal or stimulate stem cell differentiation, which  
27 may increase tumor heterogeneity.<sup>39</sup> Cells in tumor tissue differ in morphology, the quantities of vesicles,  
28 organelles, and mitochondria, density, size, and cytoskeleton arrangement. According to this, their susceptibility  
29 to ROS damage may also vary. Meanwhile, ROS is implicated in immune reactions, such as macrophage  
30 polarization and activation.<sup>40, 41</sup> As reported, the reduce of ROS inhibited repolarization of tumor associated  
31 macrophages (TAM) to M1 macrophage.<sup>42, 43</sup> Thus, ROS production played an important role in tumor  
32 microenvironment regulation and tumor characteristic. Meanwhile, as reported, on one hand, ROS can destroy  
33 mitochondrial membrane and cause apoptosis;<sup>44, 45</sup> On the other hand, for resistant cells, ROS can also inhibit  
34 the respiratory chain, reduce the generation of energy, and help to overcome energy dependent drug efflux.<sup>46</sup>  
35 What's more, delivering antitumor drugs to mitochondria usually leads to ROS production increase. Therefore,  
36 ROS amount can reflect the mitochondria targeting ability. Here, cell-permeant reagent 2',7'-  
37 dichlorodihydrofluorescein diacetate (DCFH-DA) was used to visualize ROS level. DCFH-DA travels easily across cell  
38 membrane with no significant fluorescence intensity in normal status, while once was oxidated by ROS in cells, DCFH-  
39 DA would transform into 2',7'-dichlorofluorescein (DCF) accompanied by detectable green fluorescence intensity. In  
40 Figure 4A, P-Dox and GNP-P-Dox produced little ROS, while ROS level in P-Dox-GA and GNP-P-Dox-GA treated  
41 cells was 3.09-fold and 3.33-fold higher than that of P-Dox and GNP-P-Dox treated cells, respectively. Meanwhile,  
42 no significant difference existed in the amount of ROS produced among P-Dox-GA and GNP-P-Dox-GA group, or  
43 among P-Dox and GNP-P-Dox group. All of the above results were consistent with their mitochondrial targeting  
44  
45  
46  
47  
48  
49  
50  
51  
52  
53  
54  
55  
56  
57  
58  
59  
60

abilities, indicating that the improvement of Dox mitochondrial accumulation indeed increased ROS production.

### 3.6 Overcoming multidrug resistance by high ROS level

To investigate whether the increased ROS could contribute to overcome multidrug resistance, P-gp activity and Dox efflux ratio in HepG2/ADR cells were investigated. At first, cells were treated with fresh medium or samples. After 4 h incubation, samples were replaced by calcein AM which is a substrate of P-gp for another 30 min. Stronger cellular fluorescence indicates weaker P-gp activity. Figure 4B showed that intracellular calcein fluorescence intensity in GA unmodified carrier groups was only slightly higher than control group, whereas the fluorescence intensity was enhanced by about 1.5-fold after treatment of GA modified groups (P-Dox-GA and GNPs-P-Dox-GA), indicating that GA-modification decreased P-gp activity. This may be attributed to the objective fact that GA mediated mitochondria targeting of Dox and produced more ROS, resulting in reduced P-gp activity. ROS has recently been verified to be integral to the regulation of multidrug resistance, and it regulated the oxidation of NADH into NAD<sup>+</sup> to decrease available ATP amount, following down-regulate expression of P-gp.<sup>46</sup> Therefore, the increasing of ROS level could account for the lower P-gp activity, and then increasing Dox retention in HepG2/ADR cells would happen.

Afterwards, Dox efflux ratio was evaluated by determining retained Dox fluorescence in HepG2/ADR cells. A lower efflux ratio suggested lower P-gp activity. Up to 62.5% of free Dox was pumped out of cells (Figure 4C), verifying free drugs are highly impressionable to P-glycoprotein on cell membrane through diffusion. Comparatively, the Dox efflux rate in P-Dox and GNPs-P-Dox reduced, which confirmed the previous reports,<sup>47</sup> that HPMA carriers could efficiently decrease drug efflux through endocytosis. More surprisingly, P-Dox-GA and GNPs-P-Dox-GA reduced efflux rate to 38.1% and 34.2%, which were only 61% and 55% compared with that of free Dox group, indicating the synergism of endocytosis and down-regulated expression levels of P-glycoprotein. Gelatin nanoparticles and HPMA copolymer conjugates were internalized into cells in membrane-limited organelles avoiding partition onto P-gp. Then, Dox-GA or Dox was released into cytoplasm from late endosomes and lysosomes in the cell perinuclear region (far from P-gp). As a result, the efflux ratio in these carrier groups was all lower than free Dox. Then base on the mitochondria targeting ability of GA, the released Dox-GA was delivered into mitochondria and produced more ROS (Figure 4A), which resulted in lower P-gp activity (Figure 4B). Hence, compare GA-modified and unmodified samples, the major efflux reduction (Figure 4C) should be due to the increase of ROS which was a result of GA mitochondrial targeting. All the results indicated that specifically produce ROS in mitochondria could reduce drug efflux by down-regulate activity of P-glycoprotein, which has a promising application potential in overcoming multidrug resistance.

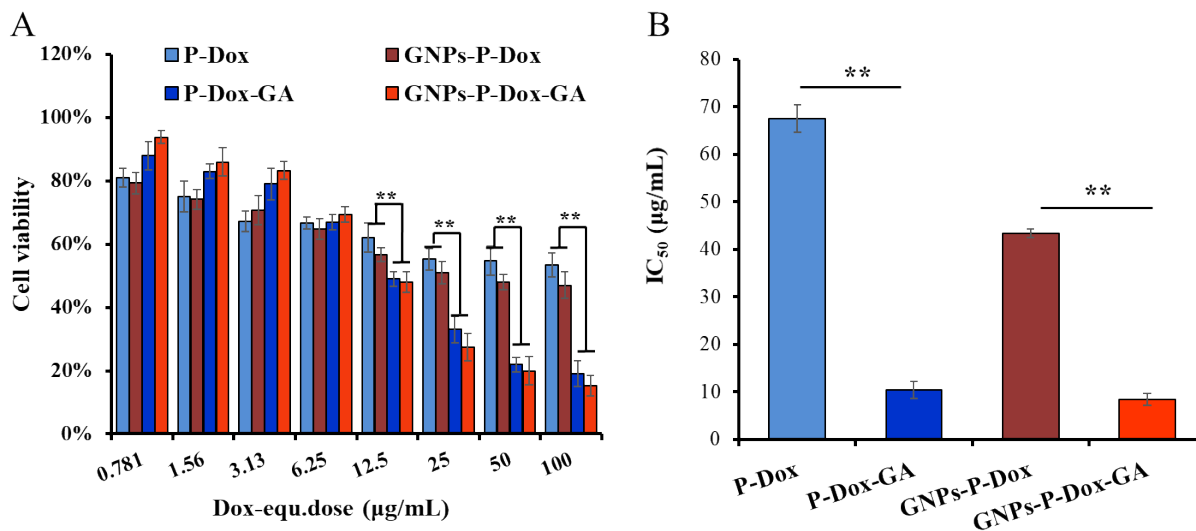


**Figure 5.** (A) HepG2/ADR cell viabilities after 48 h incubation. (B) IC<sub>50</sub> values of HPMA copolymers and gelatin nanoparticles against HepG2/ADR cells after 48 h incubation. \*\*p<0.01.

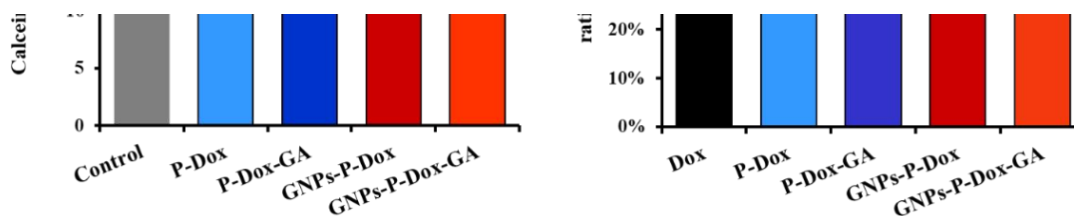


**Figure 4.** (A) ROS production in HepG2/ADR cells after 4 h incubation. (B) P-glycoprotein activity in HepG2/ADR cells after 4 h incubation. (C) Drug efflux in HepG2/ADR cells. \*\* indicated p<0.01. & and && indicated p<0.05 and p<0.01 versus control group. # and ## indicated p<0.05 and p<0.01 versus Dox group, respectively.

### 3.7 *In vitro* antitumor activity

Dox could interfere with DNA replication through inhibiting DNA topoisomerase II and gyrase enzymes, which has been selected as first-line chemotherapy for hepatocellular carcinoma.<sup>48</sup> However, most of cellular Dox would be pumped out by P-gp, which resulted in low intracellular concentration and scarce chemotherapy efficacy in drug resistant cells. The Dox cytotoxicities in HepG2 and its drug resistant cells were firstly investigated and compared. As displayed in Table S2, free Dox showed remarkable cytotoxicity in HepG2 cells (IC<sub>50</sub> = 0.18 µg/mL), whereas its antitumor activity was largely reduced in HepG2/ADR cells (IC<sub>50</sub> = 12.05 µg/mL) with resistance index (RI) of 66.94.

1  
2  
3 As reported, there was redox balance in mitochondria, which could be broken by rapidly increasing ROS levels,  
4 inducing mitochondria dysfunction and apoptosis development. Studies stated that the reductive activation of  
5 aglycone structure of Dox result in semiquinone radical formation in mitochondria, which are strong ROS that  
6 can cause cell apoptosis. Although some studies have reported that delivery systems based on polymer and  
7 nanoparticles can bypass P-gp efflux through endocytosis, the therapeutic effect of P-Dox and GNPs-P-Dox on  
8 HepG2/ADR cells was still unsatisfied (Figure 5A and 5B). Cell viability of GA modified HPMA copolymer conjugates and  
9 nanoparticle was also investigated. Excitingly, P-Dox-GA and GNPs-P-Dox-GA displayed effective antitumor activities  
10 against HepG2/ADR cells. What's more, the  $IC_{50}$  of P-Dox-GA and GNPs-P-Dox-GA were 84.5% and 80.5% lower than P-  
11 Dox and GNPs-P-Dox (Figure 5B), indicating superior cytotoxicity after GA modification. The apoptosis results on  
12 HepG2/ADR cells also demonstrated that the both P-Dox-GA and GNPs-P-Dox-GA induced more cell apoptosis after GA  
13 modification (Figure S6). In addition, there was no obvious difference in the cytotoxic effect between P-Dox-GA and  
14 GNPs-P-Dox-GA on HepG2/ADR cells, possibly due to their similar ROS production levels. However, on non-resistant  
15 HepG2 cells, GA did not significantly increase the cytotoxicity of drug carriers (Figure S7). This result implied that  
16 delivering Dox to mitochondria to reduce P-gp activity and drug efflux was a more effective strategy for drug-resistant  
17 cells than normal cells where P-gp are not overexpressed. On the whole, drug mitochondria targeting is an effective  
18 strategy for drug resistant tumor treatment.  
19  
20  
21  
22  
23  
24  
25  
26  
27  
28  
29  
30  
31  
32  
33  
34  
35  
36  
37  
38  
39  
40  
41  
42  
43  
44  
45  
46  
47  
48  
49  
50  
51  
52  
53  
54  
55  
56  
57  
58  
59  
60

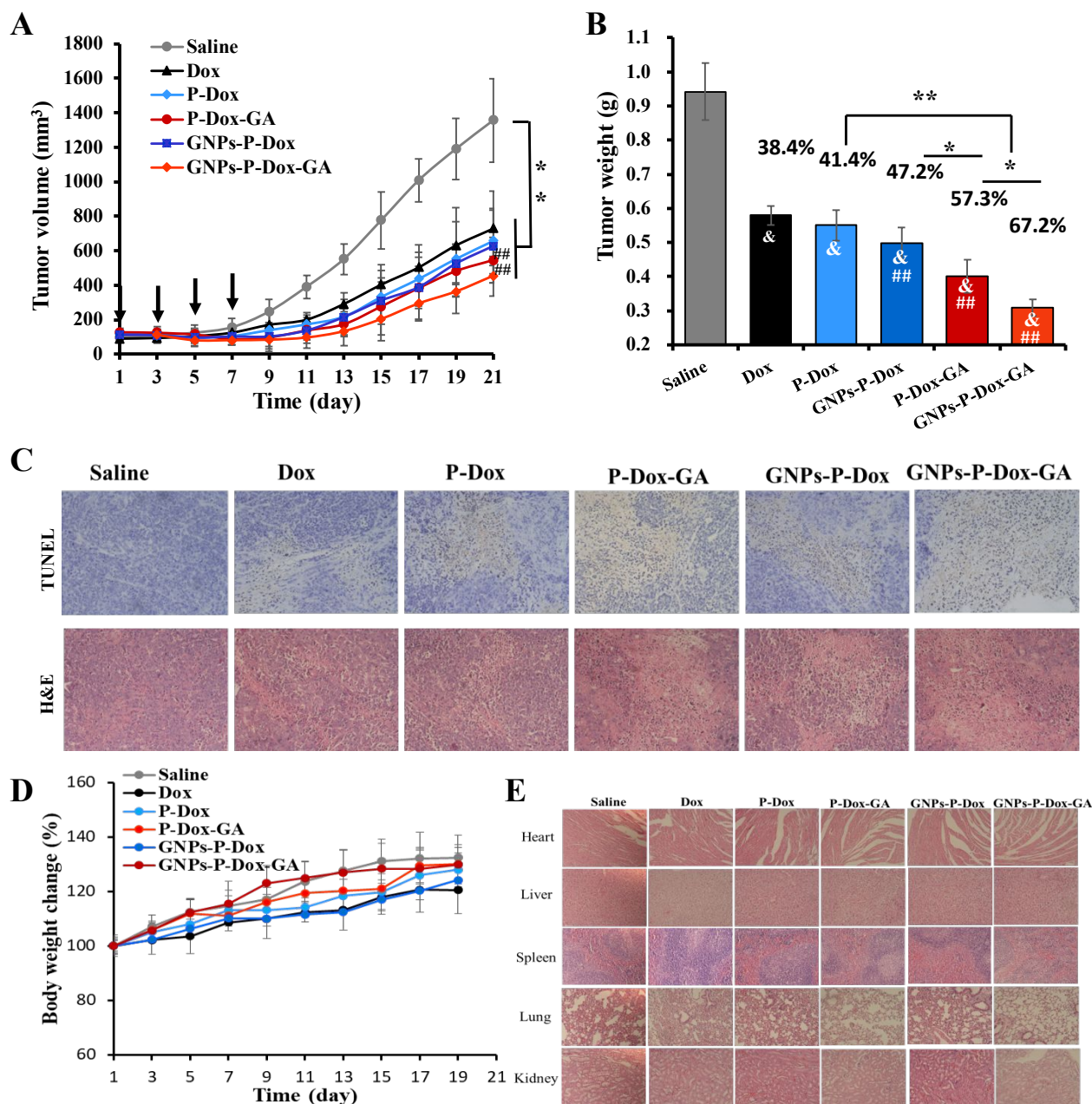


**Figure 6.** (A) Tumor growth on HepG2/ADR tumor-bearing mice for 21 days ( $n=6$ ). Arrow: saline or drug treatment. (B) Tumor weight and tumor growth inhibition rate (TGIR) calculated at the last day.  $##p<0.01$  versus free Dox.  $&p<0.01$  versus saline.  $*p<0.05$ ,  $**p<0.01$ . (C) Tumor tissues from HepG2/ADR xenografted nude mice stained by H&E (200 $\times$ ) and TUNEL (400 $\times$ ) after 21 days treatment. (D) Body weight change curves during treatment for 21 days. (E) Main organs stained by H&E staining (200 $\times$ ) after 21 days treatment.

### 3.8 *In vivo* antitumor activity

1  
2  
3 Although overcoming tumor cell MDR through enhanced ROS generation has been reported, their *in vivo*  
4 antitumor activity on MDR tumor models especially on HCC tumor model was still barely studied. Here, *in vivo*  
5 antitumor activities were evaluated on HepG2/ADR tumor bearing male nude mice, the tumor volume in saline  
6 group increased almost 13.8-fold after 21 days (Figure 6A), while the tumor growth was inhibited by all Dox  
7 carriers. The tumor growth inhibition rate (TGIR) of free Dox was only about 38.4% (Figure 6B), illustrating that  
8 the *in vivo* anticancer efficacy of free Dox was limited due to insufficient tumor accumulation and MDR in cancer  
9 cells. Although studies have demonstrated that gelatin nanoparticles and HPMA copolymer conjugates had  
10 higher tumor accumulation than free drug,<sup>21</sup> the tumor inhibition abilities of P-Dox and GNPs-P-Dox were still  
11 unsatisfactory (TGIR were 44.1% and 47.2%, respectively), which might be due to their low ROS level and *in vitro*  
12 cytotoxicity. Fortunately, compared with P-Dox, P-Dox-GA (TGIR = 57.3%) exhibited much stronger anticancer  
13 efficacy, indicating the essential of mitochondria targeting for overcoming multidrug resistance. The most  
14 significant inhibition of tumor growth was achieved by GNPs-P-Dox-GA, of which the tumor inhibition rate was up  
15 to 67.2% and 1.75-fold higher than free Dox.

16  
17  
18 Apoptosis or necrosis of tumor cells was investigated by TUNEL and H&E histochemistry. Apoptosis cells were  
19 stained to brown by TUNEL, while normal cells were stained to blue. Normal cells nuclei were stained to purple by H&E  
20 and cell plasma to pink, while necrotic cells to pink. Free Dox exhibited a modest increase in apoptosis cells and  
21 necrosis cells percentages compared to saline treated group (Figure 6C), due to poor tumor accumulation  
22 efficiency and activity in MDR cells. P-Dox and GNPs-P-Dox induced a little more apoptosis and necrosis than free  
23 Dox, while P-Dox-GA or GNPs-P-Dox-GA treated group showed significantly enhanced apoptosis and necrosis.  
24 These results clearly illustrated that P-Dox-GA and GNPs-P-Dox-GA by producing ROS in mitochondria and  
25 inducing apoptosis.

26  
27  
28 Furthermore, vital organs such as hearts, livers, spleens, lungs and kidneys did not show any histological  
29 changes (Figure 6E). Meanwhile, body weight as well as physical state of nude mice were normal after treatments  
30 (Figure 6D). These results suggested low *in vivo* toxicities of HPMA copolymer conjugates and gelatin  
31 nanoparticle-based therapy. Therefore, it is an effective strategy for drug resistant tumor treatment to deliver drugs  
32 to mitochondria.

#### 33 34 35 36 37 38 39 40 41 42 43 44 45 46 47 48 49 50 51 **4. Conclusions**

52  
53 In summary, to overcome hepatocellular carcinoma MDR, we developed a mitochondria targeting drug delivery  
54 system (GNPs-P-Dox-GA) with enhanced cellular uptake, which consists of a gelatin nanoparticle core and HPMA  
55

1  
2  
3 copolymer P-Dox-GA shell. In this study, glycyrrhetic acid (GA) was confirmed to have two abilities of hepatocellular  
4 carcinoma cells targeting and mitochondria targeting, eventually delivered doxorubicin (Dox) to mitochondria and  
5 produce a large number of ROS. Compared to non-GA modified carriers, GNPs-P-Dox-GA exhibited increased cellular  
6 uptake nearly for 4-fold and mitochondrial distribution nearly for 9-fold on drug-resistant HepG2/ADR cells, as well as  
7 increased ROS level for nearly 3-fold. More importantly, as a result, GNPs-P-Dox-GA effectively overcame the drug efflux,  
8 leading to enhanced *in vitro* anti-tumor efficiency on HepG2/ADR cells (IC<sub>50</sub> only 19.5% of unmodified ones) as well as  
9 exciting *in vivo* anti-tumor efficiency on HepG2/ADR heterotopic tumor nude mice (1.75-fold tumor growth inhibition  
10 rate than free Dox group). Based on the above advantages, the GNPs-P-Dox-GA would be promising for clinical anti-  
11 MDR treatment, and enhancing ROS generation by mitochondria targeting is an effective strategy to overcome tumor  
12 MDR.  
13  
14  
15  
16  
17  
18  
19  
20  
21  
22

### 23 **Associated Content**

### 24 **Supporting Information**

25  
26  
27 Synthesis and characterization of suc-GA, PDEA, ABIK-PDS, and SPDS. Characteristics of GNPs and GNPs-PDS.  
28 Quantitative analysis of cellular uptake in HepG2 cells. Cytotoxicity of gelatin nanoparticles against HepG2 cells.  
29 IC<sub>50</sub> of Dox against HepG2 and HepG2/ADR cells. Apoptosis in HepG2/ADR cells.  
30  
31  
32

### 33 **Author information**

34  
35 \*E-mail: huangyuan0@163.com. Tel/Fax: +86 2885501617.  
36  
37

### 38 **Notes**

39  
40 There are no conflicts to declare.  
41

### 42 **Acknowledgments**

43  
44 We acknowledge financial supports from the National Natural Science Foundation for Distinguished Young Scholars  
45 (81625023), the National Natural Science Foundation of China (81603042), and Sichuan Science and Technology  
46 Program (2018SZ0032).  
47  
48  
49  
50  
51  
52  
53  
54  
55  
56  
57  
58  
59  
60

## References

1. Zhang, Y.-K.; Wang, Y.-J.; Gupta, P.; Chen, Z.-S., Multidrug resistance proteins (MRPs) and cancer therapy. *AAPS J.* **2015**, *17*, (4), 802-812.
2. Kathawala, R. J.; Gupta, P.; Ashby Jr, C. R.; Chen, Z.-S., The modulation of ABC transporter-mediated multidrug resistance in cancer: a review of the past decade. *Drug Resist. Updates* **2015**, *18*, 1-17.
3. Chen, Z.; Shi, T.; Zhang, L.; Zhu, P.; Deng, M.; Huang, C.; Hu, T.; Jiang, L.; Li, J., Mammalian drug efflux transporters of the ATP binding cassette (ABC) family in multidrug resistance: A review of the past decade. *Cancer Lett.* **2016**, *370*, (1), 153-164.
4. Ambudkar, S. V.; Kimchi-Sarfaty, C.; Sauna, Z. E.; Gottesman, M. M., P-glycoprotein: from genomics to mechanism. *Oncogene* **2003**, *22*, (47), 7468-7485.
5. Huang, Y.; Cole, S. P.; Cai, T.; Cai, Y., Applications of nanoparticle drug delivery systems for the reversal of multidrug resistance in cancer. *Oncol. Lett.* **2016**, *12*, (1), 11-15.
6. Gupta, P.; Garg, T.; Tanmay, M.; Arora, S., Polymeric drug-delivery systems: role in P-gp efflux system inhibition. *Crit. Rev. Ther. Drug Carrier Syst.* **2015**, *32*, (3), 247-275.
7. Markman, J. L.; Rekechenetskiy, A.; Holler, E.; Ljubimova, J. Y., Nanomedicine therapeutic approaches to overcome cancer drug resistance. *Adv. Drug Delivery Rev.* **2013**, *65*, (13-14), 1866-1879.
8. Palmeira, A.; Sousa, E.; H Vasconcelos, M.; M Pinto, M., Three decades of P-gp inhibitors: skimming through several generations and scaffolds. *Curr. Med. Chem.* **2012**, *19*, (13), 1946-2025.
9. Dharmaraja, A. T., Role of reactive oxygen species (ROS) in therapeutics and drug resistance in cancer and bacteria. *J. Med. Chem.* **2017**, *60*, (8), 3221-3240.
10. Wang, H.; Gao, Z.; Liu, X.; Agarwal, P.; Zhao, S.; Conroy, D. W.; Ji, G.; Yu, J.; Jaroniec, C. P.; Liu, Z., Targeted production of reactive oxygen species in mitochondria to overcome cancer drug resistance. *Nat. Commun.* **2018**, *9*, (1), 562.
11. Kankala, R. K.; Liu, C.-G.; Chen, A.-Z.; Wang, S.-B.; Xu, P.-Y.; Mende, L. K.; Liu, C.-L.; Lee, C.-H.; Hu, Y.-F., Overcoming multidrug resistance through the synergistic effects of hierarchical pH-sensitive, ROS-generating nanoreactors. *ACS Biomater. Sci. Eng.* **2017**, *3*, (10), 2431-2442.
12. Yang, J.; Kopeček, J., The light at the end of the tunnel—second generation HPMA conjugates for cancer treatment. *Curr. Opin. Colloid Interface Sci.* **2017**, *31*, 30-42.
13. Chytil, P.; Koziolová, E.; Etrych, T.; Ulbrich, K., HPMA Copolymer–Drug Conjugates with Controlled Tumor - Specific Drug Release. *Macromol. Biosci.* **2018**, *18*, (1), 1700209.
14. Li, L.; Sun, W.; Zhong, J.; Yang, Q.; Zhu, X.; Zhou, Z.; Zhang, Z.; Huang, Y., Multistage nanovehicle delivery system based on stepwise size reduction and charge reversal for programmed nuclear targeting of systemically administered anticancer drugs. *Adv. Funct. Mater.* **2015**, *25*, (26), 4101-4113.
15. Tang, M.; Zhou, M.; Huang, Y.; Zhong, J.; Zhou, Z.; Luo, K., Dual-sensitive and biodegradable core-crosslinked HPMA copolymer–doxorubicin conjugate-based nanoparticles for cancer therapy. *Polym. Chem.* **2017**, *8*, (15), 2370-2380.
16. Zhou, Z.; Li, L.; Yang, Y.; Xu, X.; Huang, Y., Tumor targeting by pH-sensitive, biodegradable, cross-linked N-(2-hydroxypropyl) methacrylamide copolymer micelles. *Biomaterials* **2014**, *35*, (24), 6622-6635.
17. Zhou, Z.; Xu, X.; Li, L.; Huang, Y., Improvement of anti-tumor abilities on human non-small cell lung carcinoma by micellization and cross-linking of N-(2-hydroxypropyl) methacrylamide copolymers. *J. Drug Targeting* **2015**, *23*, (9), 821-831.
18. Yang, Q.; Li, L.; Sun, W.; Zhou, Z.; Huang, Y., Dual stimuli-responsive hybrid polymeric nanoparticles self-assembled from POSS-based starlike copolymer-drug conjugates for efficient intracellular delivery of hydrophobic drugs. *ACS Appl. Mater. Interfaces* **2016**, *8*, (21), 13251-13261.

19. Sharma, P. P.; Sharma, A.; Solanki, P. R., Recent Trends of Gelatin Nanoparticles in Biomedical Applications. *Adv. Nanomater.*, Springer: 2016; 365-381.
20. Forsyth, P.; Wong, H.; Laing, T.; Rewcastle, N.; Morris, D.; Muzik, H.; Leco, K.; Johnston, R.; Brasher, P.; Sutherland, G., Gelatinase-A (MMP-2), gelatinase-B (MMP-9) and membrane type matrix metalloproteinase-1 (MT1-MMP) are involved in different aspects of the pathophysiology of malignant gliomas. *Br. J. Cancer* **1999**, *79*, (11), 1828-1835.
21. Liu, Y.; Li, L.; Li, L.; Zhou, Z.; Wang, F.; Xiong, X.; Zhou, R.; Huang, Y., Programmed drug delivery system based on optimized "size decrease and hydrophilicity/hydrophobicity transformation" for enhanced hepatocellular carcinoma therapy of doxorubicin. *Nanomedicine: Nanotechnology, Biology and Medicine* **2018**, *14*, (4), 1111-1122.
22. T Madak, J.; Neamati, N., Membrane permeable lipophilic cations as mitochondrial directing groups. *Curr. Trends Med. Chem.* **2015**, *15*, (8), 745-766.
23. Lu, P.; Bruno, B. J.; Rabenau, M.; Lim, C. S., Delivery of drugs and macromolecules to the mitochondria for cancer therapy. *J. Controlled Release* **2016**, *240*, 38-51.
24. Liu, Y.; Li, Q.; Xiong, X.; Zhou, Z., Improved mitochondrial targeting effect of HPMA copolymer by SS20 peptide mediation and nonendocytosis pathway. *J. Pept. Sci.* **2019**, *25*, (2), e3144.
25. Liu, Y.; Li, Q.; Xiong, X.; Huang, Y.; Zhou, Z., Mitochondria-targeting and cell-penetrating peptides-co-modified HPMA copolymers for enhancing therapeutic efficacy of  $\alpha$ -tocopheryl succinate. *J. Mater. Chem. B* **2018**, *6*, (46), 7674-7683.
26. Sun, W.; Li, L.; Li, L.-j.; Yang, Q.-q.; Zhang, Z.-r.; Huang, Y., Two birds, one stone: dual targeting of the cancer cell surface and subcellular mitochondria by the galectin-3-binding peptide G3-C12. *Acta Pharmacol. Sin.* **2017**, *38*, (6), 806-822.
27. Ying, T.-H.; Tsai, J.-H.; Wu, T.-T.; Tsai, M.-T.; Su, W.-W.; Hsieh, Y.-S.; Liu, J.-Y., Immunochemical localization of protein kinase C alpha in the biopsies of human hepatocellular carcinoma. *Chin. J. Physiol.* **2008**, *51*, (5), 269-274.
28. Yang, L.; Yang, Z.; Jixiong, H.; Huang, S.; Deng, X.; Miao, X., Significance of the expression of glutameta decarboxylase 65 and protein kinase C in primary hepatocarcinoma tissues. *Chin. J. Gen. Surg.* **2001**, (8), 590-593.
29. Wu, F.; Li, X.; Jiang, B.; Yan, J.; Zhang, Z.; Qin, J.; Yu, W.; Gao, Z., Glycyrrhetic acid functionalized nanoparticles for drug delivery to liver cancer. *J. Biomed. Nanotechnol.* **2018**, *14*, (11), 1837-1852.
30. Zhang, C.; Liu, Z.; Zheng, Y.; Geng, Y.; Han, C.; Shi, Y.; Sun, H.; Zhang, C.; Chen, Y.; Zhang, L., Glycyrrhetic acid functionalized graphene oxide for mitochondria targeting and cancer treatment in vivo. *Small* **2018**, *14*, (4), 1703306.
31. Kroemer, G.; Galluzzi, L.; Brenner, C., Mitochondrial membrane permeabilization in cell death. *Physiol. Rev.* **2007**, *87*, (1), 99-163.
32. Etrych, T.; Mrkvan, T.; Chytil, P.; Koňák, Č.; Říhová, B.; Ulbrich, K., N - (2 - hydroxypropyl) methacrylamide - based polymer conjugates with pH - controlled activation of doxorubicin. I. New synthesis, physicochemical characterization and preliminary biological evaluation. *J. Appl. Polym. Sci.* **2008**, *109*, (5), 3050-3061.
33. Zeng, X.; Zhang, Y.; Nyström, A. M., Endocytic uptake and intracellular trafficking of bis-MPA-based hyperbranched copolymer micelles in breast cancer cells. *Biomacromolecules* **2012**, *13*, (11), 3814-3822.
34. Song, Q.; Li, D.; Zhou, Y.; Yang, J.; Yang, W.; Zhou, G.; Wen, J., Enhanced uptake and transport of (+)-catechin and (-)-epigallocatechin gallate in niosomal formulation by human intestinal Caco-2 cells. *Int. J. Nanomed.* **2014**, *9*, 2157-2165.
35. Banerji, S.; Wright, A. J.; Noble, M.; Mahoney, D. J.; Campbell, I. D.; Day, A. J.; Jackson, D. G., Structures of the Cd44-hyaluronan complex provide insight into a fundamental carbohydrate-protein interaction. *Nat. Struct. Mol. Biol.* **2007**, *14*, (3), 234-239.
36. Schanté, C. E.; Zuber, G.; Herlin, C.; Vandamme, T. F., Chemical modifications of hyaluronic acid for the synthesis of derivatives for a broad range of biomedical applications. *Carbohydr. Polym.* **2011**, *85*, (3), 469-489.
37. Tian, Q.; Wang, X.; Wang, W.; Zhang, C.; Liu, Y.; Yuan, Z., Insight into glycyrrhetic acid: the role of the hydroxyl group on liver targeting. *Int. J. Pharm.* **2010**, *400*, (1-2), 153-157.

- 1  
2  
3 38. Wang, X.; Gu, X.; Wang, H.; Sun, Y.; Wu, H.; Mao, S., Synthesis, characterization and liver targeting evaluation of self-  
4 assembled hyaluronic acid nanoparticles functionalized with glycyrrhetic acid. *Eur. J. Pharm. Sci.* **2017**, *96*, 255-262.
- 5 39. de Sá Junior, P. L.; Câmara, D. A. D.; Porcacchia, A. S.; Fonseca, P. M. M.; Jorge, S. D.; Araldi, R. P.; Ferreira, A. K., The  
6 roles of ROS in cancer heterogeneity and therapy. *Oxid. Med. Cell. Longevity* **2017**, 2017, Article ID 2467940.
- 7  
8 40. Tan, H.-Y.; Wang, N.; Li, S.; Hong, M.; Wang, X.; Feng, Y., The reactive oxygen species in macrophage polarization:  
9 reflecting its dual role in progression and treatment of human diseases. *Oxid. Med. Cell. Longevity* **2016**, 2016, Article ID  
10 2795090.
- 11  
12 41. Nathan, C.; Cunningham-Bussel, A., Beyond oxidative stress: an immunologist's guide to reactive oxygen species. *Nat.*  
13 *Rev. Immunol.* **2013**, *13*, (5), 349.
- 14  
15 42. Lee, A. S.; Jung, Y. J.; Kim, D.; Nguyen-Thanh, T.; Kang, K. P.; Lee, S.; Park, S. K.; Kim, W., SIRT2 ameliorates  
16 lipopolysaccharide-induced inflammation in macrophages. *Biochem. Biophys. Res. Commun.* **2014**, *450*, (4), 1363-1369.
- 17  
18 43. Padgett, L. E.; Burg, A. R.; Lei, W.; Hubert, M. T., Loss of NADPH oxidase-derived superoxide skews macrophage  
19 phenotypes to delay type 1 diabetes. *Diabetes* **2015**, *64*, (3), 937-946.
- 20  
21 44. Simon, H.-U.; Haj-Yehia, A.; Levi-Schaffer, F., Role of reactive oxygen species (ROS) in apoptosis induction. *Apoptosis*  
22 **2000**, *5*, (5), 415-418.
- 23  
24 45. Indran, I. R.; Tufo, G.; Pervaiz, S.; Brenner, C., Recent advances in apoptosis, mitochondria and drug resistance in cancer  
25 cells. *Biochim. Biophys. Acta, Bioenerg.* **2011**, *1807*, (6), 735-745.
- 26  
27 46. Pelicano, H.; Carney, D.; Huang, P., ROS stress in cancer cells and therapeutic implications. *Drug Resist. Updates* **2004**,  
28 *7*, (2), 97-110.
- 29  
30 47. Minko, T.; Kopečková, P.; Pozharov, V.; Kopeček, J., HPMA copolymer bound adriamycin overcomes MDR1 gene  
31 encoded resistance in a human ovarian carcinoma cell line. *J. Controlled Release* **1998**, *54*, (2), 223-233.
- 32  
33 48. Deng, G.-L.; Zeng, S.; Shen, H., Chemotherapy and target therapy for hepatocellular carcinoma: New advances and  
34 challenges. *World J. Hepatol.* **2015**, *7*, (5), 787-798.
- 35  
36  
37  
38  
39  
40  
41  
42  
43  
44  
45  
46  
47  
48  
49  
50  
51  
52  
53  
54  
55  
56  
57  
58  
59  
60

For Table of Contents Only

# Enhanced Reactive Oxygen Species Generation by Mitochondria Targeting of Anti-cancer Drug to Overcome Tumor Multidrug Resistance

Yuanyuan Liu<sup>#</sup>, Zhou Zhou<sup>#</sup>, Xi Lin, Xiaofeng Xiong, Rui Zhou, Minglu Zhou, Yuan Huang<sup>\*</sup>

Key Laboratory of Drug Targeting and Drug Delivery System, Ministry of Education, West China School of Pharmacy, Sichuan University, No. 17, Block 3, Southern Renmin Road, Chengdu 610041, P. R. China.

<sup>#</sup> These authors contributed equally to this work.

